Supporting Online Information for

On-Chip Rayleigh Imaging and Spectroscopy of Carbon Nanotubes

Daniel Y. Joh[1,2], Lihong H. Herman[1], Sang-Yong Ju[2], Jesse Kinder[2], Michael A. Segal[2], Jeffreys N. Johnson[2], Garnet K. L. Chan[2], and Jiwoong Park[2,3,†]

[1]School of Applied and Engineering Physics, Cornell University, Ithaca, NY, 14853 USA

[2]Department of Chemistry and Chemical Biology, Cornell University, Ithaca, NY, 14853 USA

[3]Kavli Institute at Cornell for Nanoscale Science, Cornell University, Ithaca, NY, 14853 USA

[†]To whom correspondence should be addressed. Email: jpark@cornell.edu

Supplementary Information Contents

1. Device Fabrication

All fabrication was performed using conventional photolithography on commercially available ST-cut quartz wafers (Hoffman Materials, LLC). A reactive-ion etching system was used to etch alignment marks 400 nm deep. The wafers were diced and substrates were placed in a quartz reaction tube and annealed in air at 900^{o}C for 9 hours. The catalyst pattern was then defined by photolithography, and 2 Å of Fe was evaporated onto individual substrates. Following lift off, aligned SWNTs were grown using a procedure adapted from Kocabas *et al.* (*Small* **1**, 1110 (2005)) at 865^{o}C using methane as the carbon feedstock.

2. Sample Preparation for Rayleigh imaging

First, cover glasses (Corning, No.1, 22 mm squares) were rigorously cleaned by placing them in a 3:1 mixture of H_2SO_4: H_2O_2 at 90^{o}C for 30 min and subsequently rinsing them with deionized water and isopropyl alcohol, followed by drying under a flow of N_2. Next, the SWNT substrate was placed in a quartz reaction tube and annealed at 275^{o}C under a constant flow of H_2 (350 sccm) and Ar (500 sccm) for 10 minutes. Finally, a drop of glycerol (Sigma-Aldrich, $\geq$ 99.5 % spectrophotometric grade) preheated to 100^{o}C was applied between the SWNT substrate and coverglass and held together by Scotch tape.

3. Atomic Force Microscopy

To make optical vs. AFM comparisons (such as those shown in Fig. S4), we first located SWNTs on the sample using our optical setup. Using the pre-patterned alignment

marks on the substrates as guides, we subsequently obtained AFM images and diameters after taking extra care to remove the glycerol from the sample (since residual glycerol can significantly affect the AFM measurement). To remove the glycerol, the sample was first soaked for a full day in ethanol, and then thoroughly rinsed with deionized water, acetone, and finally isopropanol. After drying the substrate with N_2, the sample was placed in a quartz tube and annealed at 300^o C for at least 15 minutes under a constant flow of H_2 (300 sccm) and Ar (500 sccm) to eliminate any residual glycerol or solvents. The sample was then taken to the AFM for imaging and height analysis.

AFM imaging was performed in air using a commercial MFP3D AFM (Asylum Research, Santa Barbara, CA) in tapping mode with free oscillating amplitude of 71 nm and set point of 52 nm for all measurements. Diameter measurements were performed in repulsive mode ($\phi < 90^o$) with a scanning rate of 1Hz and scan size of ~1μm. 300 kHz aluminum-coated SiO_2 cantilevers (Budget Sensors, Bulgaria) were purchased from Ted Pella Inc. SWNT diameter was determined by fitting AFM height traces to a Gaussian function and averaging the fitted amplitudes of several measurements (> 3)

4. Experimental Apparatus for On-Chip Rayleigh Imaging

Detailed schematic of the experimental apparatus is shown in Fig. S1. The quartz substrate containing aligned SWNTs was coated with glycerol, whose refractive index is similar to that of quartz. The broadband excitation laser (L) is linearly polarized (P) and the wavelength and bandwidth are controlled by a monochromator (M). The excitation laser is introduced into the sample at an angle using a darkfield condenser (DCW) and reflected completely at the uppermost quartz-air interface by total internal reflection,

preventing the exciting laser from entering the detection optics. The total laser power at the sample varies between 0.1 mW and 1 mW (depending on the wavelength) using a typical bandwidth of 20 nm. The scattered light is collected by a high numerical aperture objective lens (OL) (N.A. = 0.95) and focused onto a 2D array detector (CCD) (Sensicam QE, Cooke Corporation) via tube lens (TL).

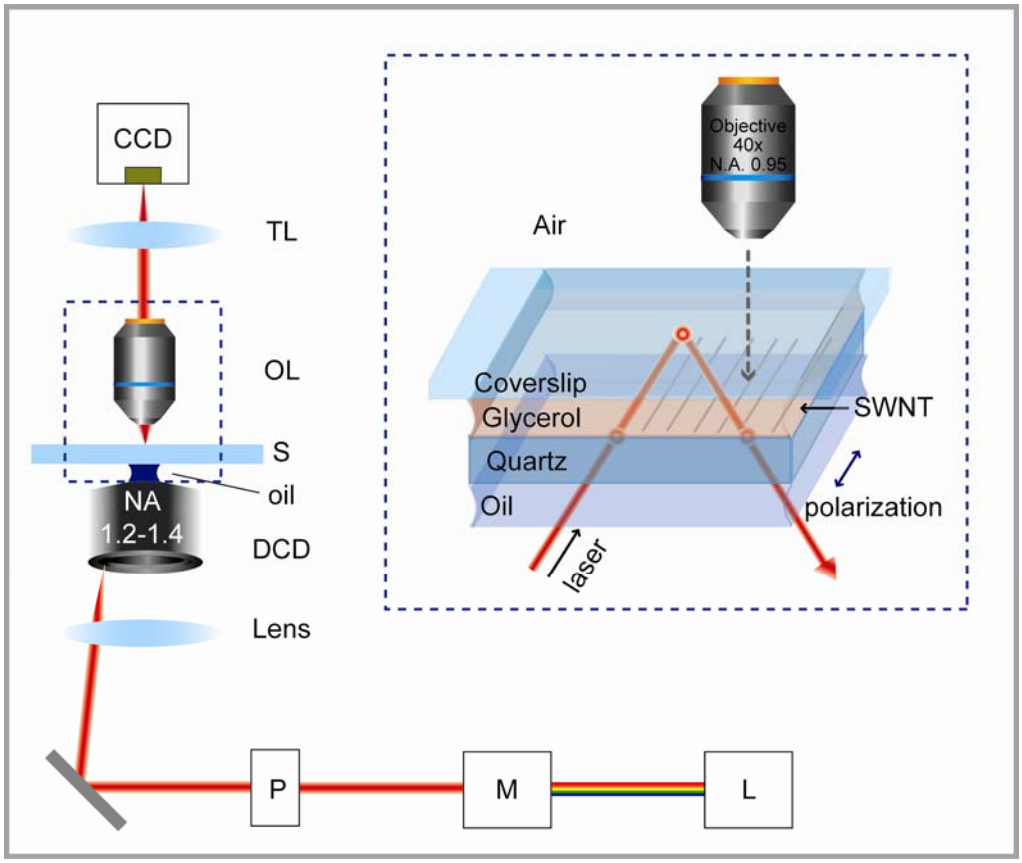

Figure S1. Schematic of on-chip Rayleigh imaging setup. See text above for abbreviations.

5. Confirmation of Rayleigh Scattering Signal

Using the geometry described in Fig. S1, images were taken using a CCD camera with and without a bandpass filter (bandwidth < 10 nm) in the detection pathway

matching the excitation wavelength (bandwidth < 5nm) with exposure time of 7 seconds (see Fig. S2). These images confirm that the majority of the collected photons are due to the elastic scattering of SWNTs, as opposed to Raman scattering or photoluminescence. The scattering intensity with and without a bandpass filter (I_F and I_o, respectively) were measured, and their ratio was typically $I_F / I_o \approx 0.61$, similar to the transmission of the bandpass filter.

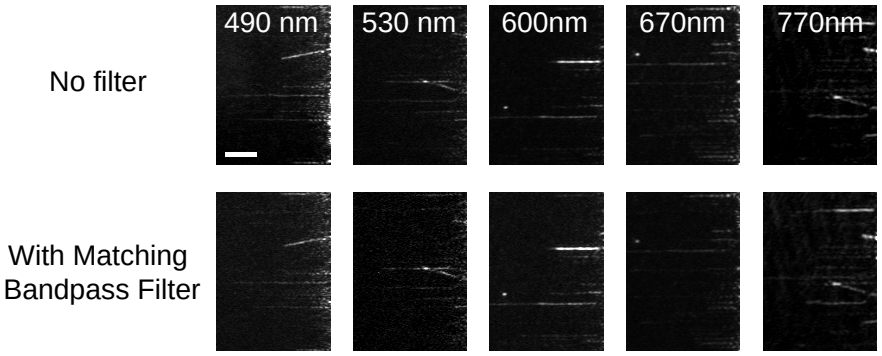

Fig. S2: CCD Images with and without matching bandpass filters. Black and white images taken with and without a bandpass filter (bandwidth < 10 nm) matching the excitation wavelength in the detection pathway. Scale bar, 5 μm

6. Normalization and Construction of Rayleigh Images and Spectra

Below we show plots for the quantum efficiency of the CCD camera (Fig. S3a) and for the wavelength-dependence of the excitation laser power before it hits the sample (i.e. after monochromator and additional optical elements) (Fig. S3b). For the wavelength range of our experiment, the traces of both graphs do not change very rapidly. As a result, within our experimental peak width (~100 meV), we can assume very slow change, and thus the wavelength-dependence of the detection efficiency and excitation profile will not affect the lineshapes of the SWNT resonance significantly.

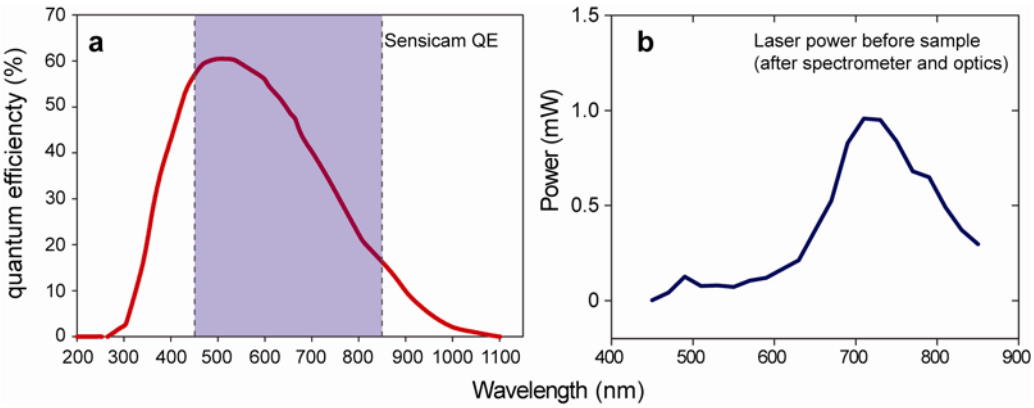

Figure S3: Wavelength-dependence of excitation and detection elements. Quantum efficiency of the CCD camera (**a**) and profile of the excitation laser before hitting the sample (**b**) as a function of wavelength. The wavelength range used in this experiment is highlighted in blue.

The Rayleigh images and spectra for SWNTs are constructed using a frame-by-frame calibration protocol. The dark current count was first subtracted from each frame. To correct for the background due to out-of-plane scattering and autoflourescence of the medium, we applied a background subtraction/low-pass spatial filter using the image processing software ImageJ (Rasband, W.S., ImageJ, U. S. National Institutes of Health). Next, to calibrate for the detection efficiency of the detector and changes in the excitation laser all as a function of wavelength, each frame was divided by the spatial profile of the illumination fitted to a 2D Gaussian. This resulted in each frame (which corresponds to a particular wavelength) being calibrated for wavelength-dependent fluctuations in the camera and excitation laser while normalizing the overall intensity for each frame.

Since each frame (out of the total 200) represents a 2 nm step, each pixel comprising the composite spatial image (also commonly known as an "image stack") of

the illuminated area (approximately 70× 80 μm^2) corresponds to a spectral profile. To extract spectral profiles for SWNTs, we traced the integrated light intensity per unit length measured from the pixels in the image stack in which SWNTs appeared using ImageJ.

7. Rayleigh Imaging-AFM Correspondence

We compared our optical images to their corresponding AFM images in order to confirm that SWNTs on the substrate were visible under our Rayleigh imaging scheme. Fig. S4 shows a representative colour Rayleigh images compared to an AFM images of the same area.

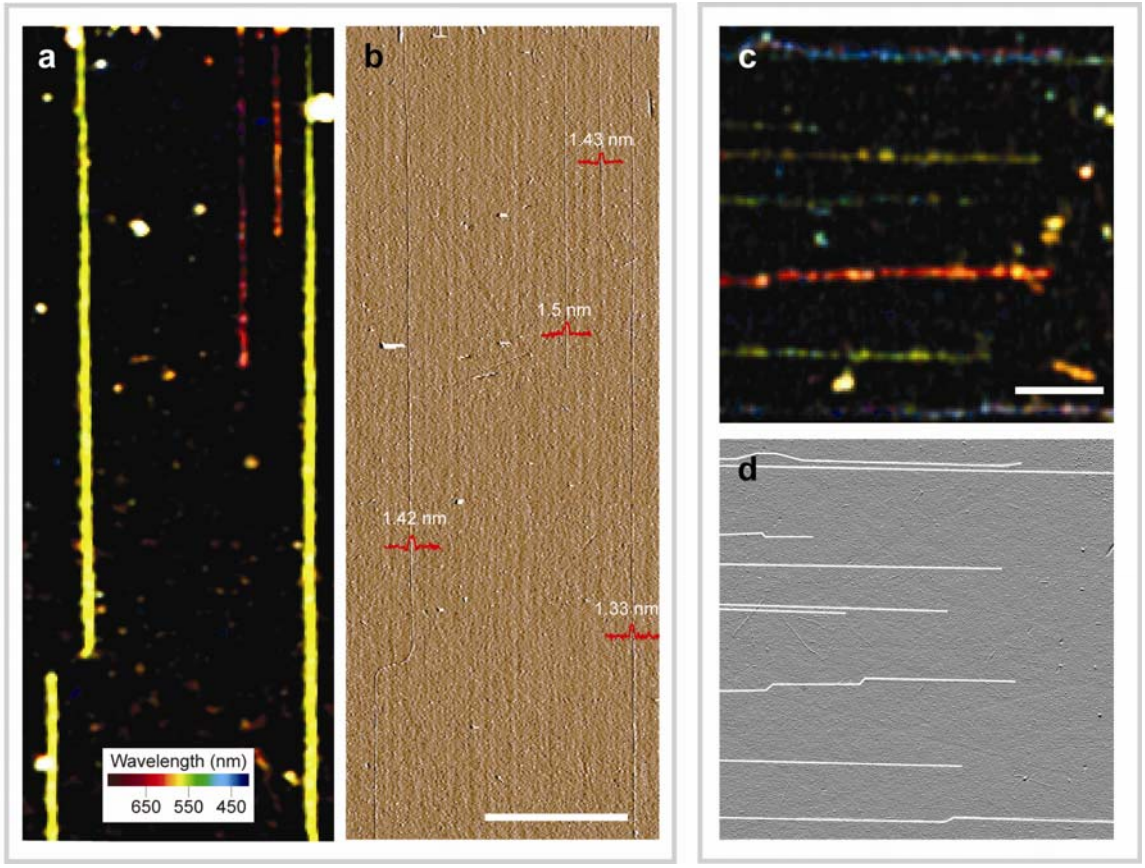

Figure S4. Correspondence between Rayleigh and AFM Imaging. a, b, Color Rayleigh image (**a**) and matching AFM image (**b**). Scale bar, 10 μm. **c, d,** Color Rayleigh image (**c**) and matching AFM image (**d**) for a different region. For the AFM image in (**d**), the SWNTs are outlined in white for clarity. Scale bar, 5 μm.

8. Diameter Distribution of SWNTs

Fig. S5 shows the diameter distributions we measured for the SWNTs studied in our sample. The distribution in (**a**) is centred at 1.2 ± 0.5 nm, ranging from 0.5 nm to 2.2 nm.

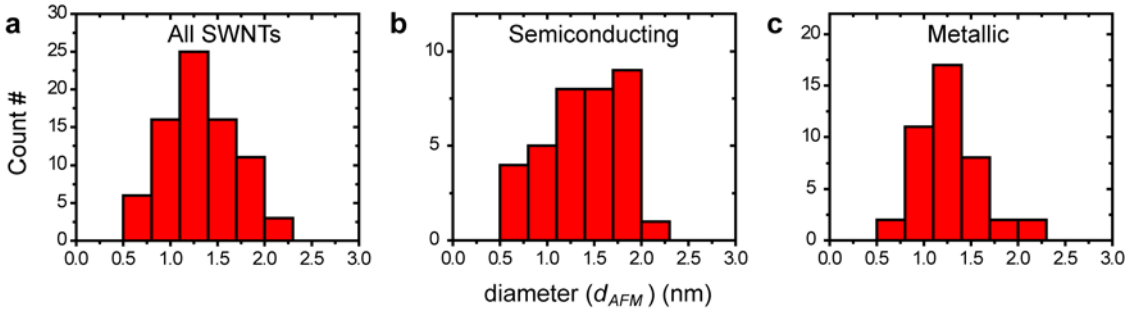

Figure S5. Diameter Distribution of typical SWNT sample. a, b, c, Diameter distribution (d_{AFM}) for all SWNTs studied (**a**), semiconducting SWNTs (**b**), and metallic SWNTs (**c**).

9. Optical Response of Multi-Walled vs. Single-Walled Carbon Nanotubes

SWNTs can easily be distinguished from MWNTs from their distinct optical spectra. For instance, the MWNT shown in the Rayleigh image in Fig. S6a has a broad optical

response (as shown by its Rayleigh spectrum in Fig. S6c), whereas the SWNT exhibits a single sharp peak in its Rayleigh scattering spectrum (Fig. S6b).

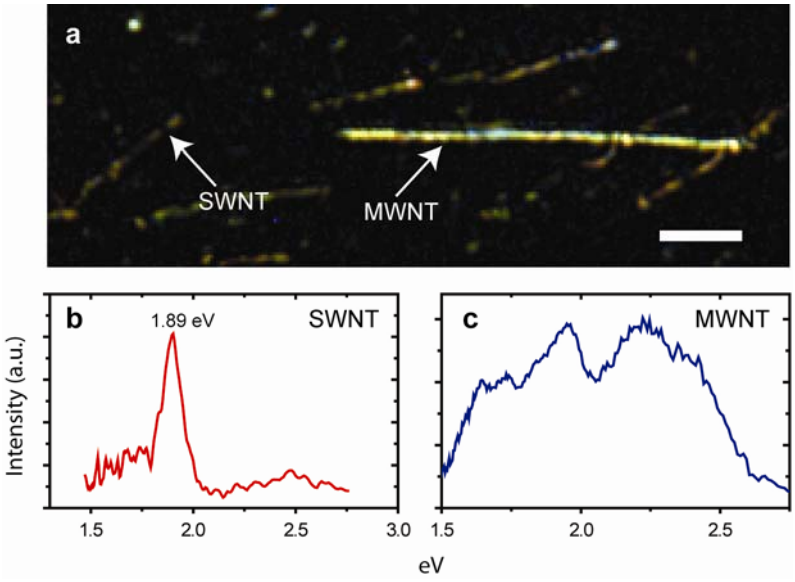

Figure S6. SWNT Optical Response versus that of MWNTs. a, Color Rayleigh image of randomly dispersed nanotube growth. Arrows indicate a SWNT and MWNT. **b, c,** Corresponding Rayleigh spectra of the SWNT (**b**) and MWNT (**c**)

10. Shifts in Rayleigh Peak Position and Intensity in SWNT Bundles (Main Text Fig. 4a-c)

Shown in Fig. 4 of the main text is a pair of nanotubes that are initially isolated, then run parallel with a separation distance of 75 nm, and finally become bundled. Fig. S7a illustrates this configuration. Fig. S7b plots the shift in peak position (denoted by ΔE) for SWNTs α and β as a function of gap distance for the regions marked by the symbols, and Fig. S7c plots the normalized intensity as a function of gap distance between the tubes.

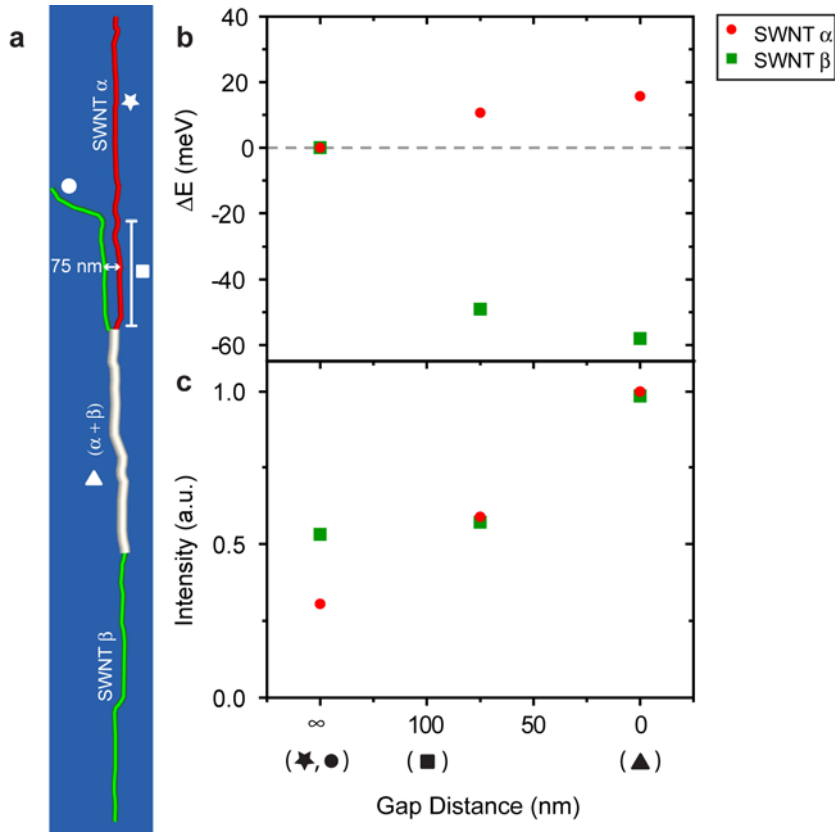

Figure S7. Energy Shift and Intensity vs. Gap Distance. a, Illustration depicting the bundling configuration for SWNTs α and β. **b,** Shift in Rayleigh scattering peak position (ΔE) versus gap distance between the tubes. **c,** Normalized Rayleigh scattering intensity versus gap distance between the tubes.

11. Additional SWNT Bundling Example

We were furthermore able to probe the effects of intertube coupling for nanotubes in a slightly different geometry than that shown in Fig. 4. Fig. S8a shows the Rayleigh image of two SWNTs (δ and γ) forming a bundle in the region indicated by the dashed red lines (close-up AFM image of the bundling junction shown in the inset of Fig. S8b). The nanotubes remain bundled in the region marked by ($\delta + \gamma$) and eventually SWNT γ

stops abruptly at the location marked by the white arrow. The peak scattering intensity SWNT δ in its bundled state is significantly larger compared to when it is isolated. The point at which SWNT δ is no longer bundled was determined by examining the intensity of the Rayleigh scattering signal along the nanotube axis. In addition, we observe that the spectral peak for SWNT δ is redshifted by about 10 meV when it is the bundled state. The increase in scattering intensity and magnitude of the redshift in the Rayleigh scattering peak are consistent with Rayleigh scattering measurements performed in air on bundled nanotubes suspended across lithographically defined slits (*Phys. Rev. Lett.* **96**, 167401).

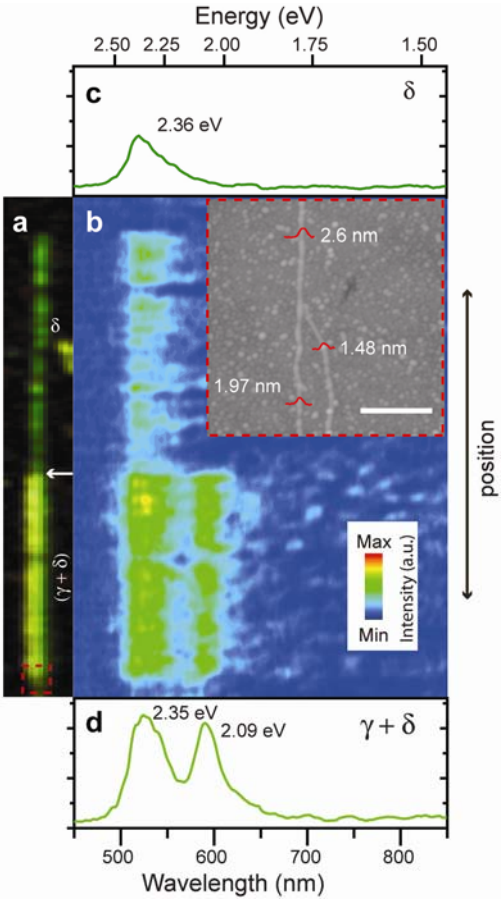

Figure S8. SWNT Bundling. **a,** Rayleigh image of a nanotube bundle comprised of SWNTs δ and γ. The tubes are bundled in the region marked by (δ + γ) until the

location marked by the white arrow, at which point SWNT δ outgrows SWNT γ. Scale bar, 5 μm. **b,** Contour plot of the optical response as a function of excitation wavelength along nanotube axis. Inset: Enlarged AFM image of the bundling junction, denoted in the Rayleigh image (**a**) by the dashed red box. Scale bar, 500 nm. **c, d,** Normalized Rayleigh scattering spectra for isolated SWNT δ (**c**) and bundled SWNTS ($\delta + \gamma$) (**d**).

12. Confocal Raman Setup

Raman spectra were obtained using a custom-built confocal Raman setup using an inverted microscope (Olympus IX71) as the main platform. The excitation diode laser centered at 632.8 nm. Scattered Raman signals were collected using a backscattering geometry as shown in Figure S6. Collected signals were analyzed using gratings of either 300g/mm or 1200g/mm for spatial 2D and point imaging, respectively. The spectral wavelength was calibrated using a Si substrate as an external reference.

Details of Raman setup: The Raman setup was built on a vibration-isolated optical table in a room isolated from external light. The schematic in Figure S6 illustrates the experimental apparatus for confocal Raman spectroscopy. A temperature- and power-controlled diode laser (632.8 nm, P_{max} = 35 mW, Thorlabs) was used as the excitation source. The beam was linearly polarized, collimated, and directed towards the back aperture of a 50× objective (UMPlanFL, NA = 0.8, Olympus). The bandwidth of the excitation wavelength is further narrowed via double bandpass filter (632.8 nm, O.D. > 5, bandwidth = 2.4 nm, Semrock). The collimated laser light was focused onto our sample

containing aligned nanotubes. The sample was mounted onto LabVIEW-controlled XYZ stage (scxyz100 piezo stage, Thorlabs). The polarization cube (CM1-PBS1, Thorlabs) and notch filter (632.8 nm, O.D. > 6, bandwidth = 266 cm^{-1}, Kaiser Optical System) were used to reject superfluous scattered light and the majority of the excitation laser, respectively, before Raman signals reached spectrometer (SP2300i, Princeton Instruments), which was connected to the sideport of the microscope. Randomly scattered light was further eliminated by a kinematic slit (ca. 100 μm) and the Raman signal was recorded using a CCD camera (PIXIS 400, Princeton Instruments).

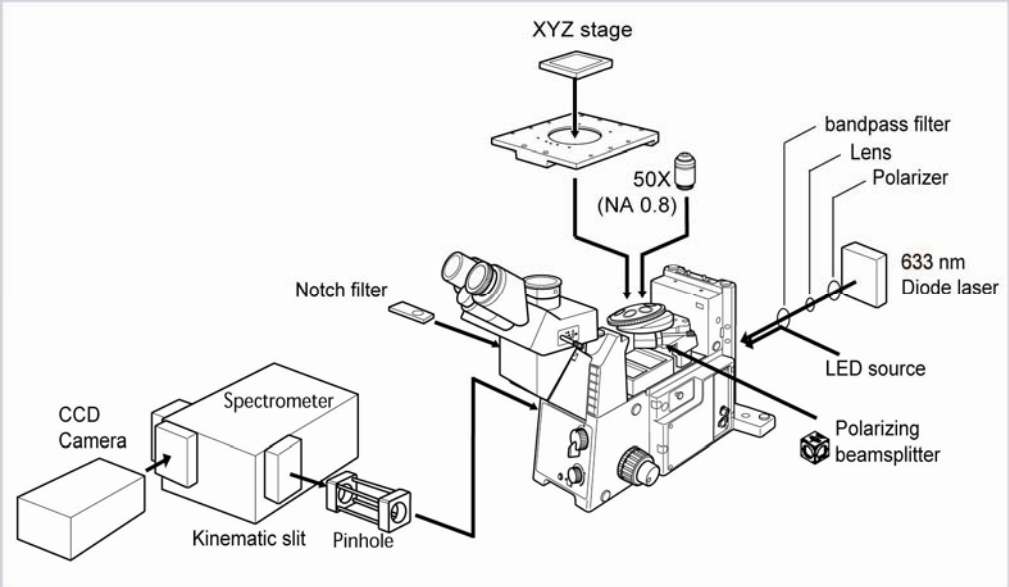

Figure S9. Schematic of Raman setup. Part of the figure was adapted from Olympus IX71 manual.